Excimer Laser Projection Micromachining of Polyimide Thin Films Annealed at Different Temperatures

Xiang Zhang, Costas P. Grigoropoulos, Douglas J. Krajnovich, and Andrew C. Tam, *Senior Member, IEEE*

Abstract—A KrF excimer laser projection micromachining tool has been designed and implemented aiming to accomplish one-step etching with micron resolution for applications such as chip module packaging and polyimide technology in semiconductor manufacturing. Two polyimide (Probimide® 7020) thin films spun on the silicon wafers are annealed at 100 °C and 400 °C, respectively, in order to investigate the effect of the annealing temperature on the laser micromachining process. The micromachined polyimide surface morphology is studied by scanning electron microscopy (SEM), atomic force microscopy (AFM), and a surface profilometer for determination of the etch rate at different laser fluences. Micromachining with micron resolution is achieved by this excimer laser projection tool. Measured on a 25 μm line, the etch rate dependence on laser fluence both below and above the ablation threshold is investigated over the fluence range from 10–1000 mJ/cm^2. The polyimide thin film optical properties, i.e., the components of the complex refractive index, n and k at λ = 248 nm are measured by a spectroscopic ellipsometer for both films. The etch rate above the ablation threshold for the film annealed at 100 °C is found 60% higher than that for the film annealed at 400 °C. This behavior originates from the correspondingly higher by 82% absorption coefficient, α in the 100 °C film. The ablation thresholds for both films are found the same at about 100 mJ/cm^2. Calculated etch rates agree with experimental values within 15%. Etch rates of the order of nanometer can be achieved near the ablation threshold of 100 mJ/cm^2 for both films. The linearity between the etched depth and the number of the laser pulses prevails for the micromachining process at and above the threshold.

I. INTRODUCTION

AS AN EMERGING technology in microelectronics and micromechanics, excimer laser micromachining is becoming more and more attractive to the microelectronics manufacturing due to its unique noncontact and one-step process features [1]–[4]. It emerges as either a complementary or a competing process to existing micro fabrication technologies such as ion milling and plasma etching. Since most materials are strong absorbers to UV wavelength radiation, the excimer laser light is absorbed in a very shallow region near

the irradiated material surface. On the other hand, the very short duration of the laser pulse brings the peak power up to 10^{10} W/cm^2. These two unique features make the excimer laser a successful tool for initiating photochemical and/or photothermal ablation, leading to precision micromachining for surface patterning [5]–[7], chemical or physical modification [8]–[12], and via hole formation in electronic circuit packaging [13]. Given that photons can be regarded as "clean particles" and since the laser irradiation is essentially a noncontact process, excimer laser micromachining can be accomplished in air instead of in vacuum as in the case for plasma etching or ion milling, thus eliminating foreign chemical contamination.

Excimer laser micromachining on polymer films has been studied extensively due to its technological importance in microelectronics and micromechanics applications [5], [8], and [14]–[17]. Due to its low dielectric constant, polyimide films are often used to insulate the different circuit layers in semiconductor chip packaging modules. Conventionally, the via hole fabrication in the polyimide films for interconnecting the different layers in a chip package module must go through several lithographic steps such as exposure, developing, wet etch, plasma etching or ion milling [13]. However, excimer laser micromachining is a one-step ablation process and its shorter wavelength can give better patterning resolution than the mercury arc lamp exposure used in conventional lithography. Excimer laser micromachining may also have an impact on the development of polyimide technology for electronic device applications. As a promising alternative to silicon oxide, polyimide films have comparable physical and chemical properties as excellent insulating layers between metallic interconnects and diffusion barriers for selective doping. Annealed polyimide films also have reasonable mechanical properties. By a spin-on process, the polyimide planarization can be very simple and cost-effective, compared with the relatively high temperature CVD or sputtering for growing or depositing silicon oxide layers which both require sophisticated vacuum and mass flow control systems. By projecting a laser mask through the optical imaging system, the excimer laser ablation provides a direct way for parallel micromachining of the polyimide thin films in air. Conventional steps in oxide etching ranging from lithographic masking, wet etching, and/or plasma etching can be replaced by the excimer laser micromachining, resulting in great process simplification and correspondingly low equipment cost. The excimer laser micromachining can
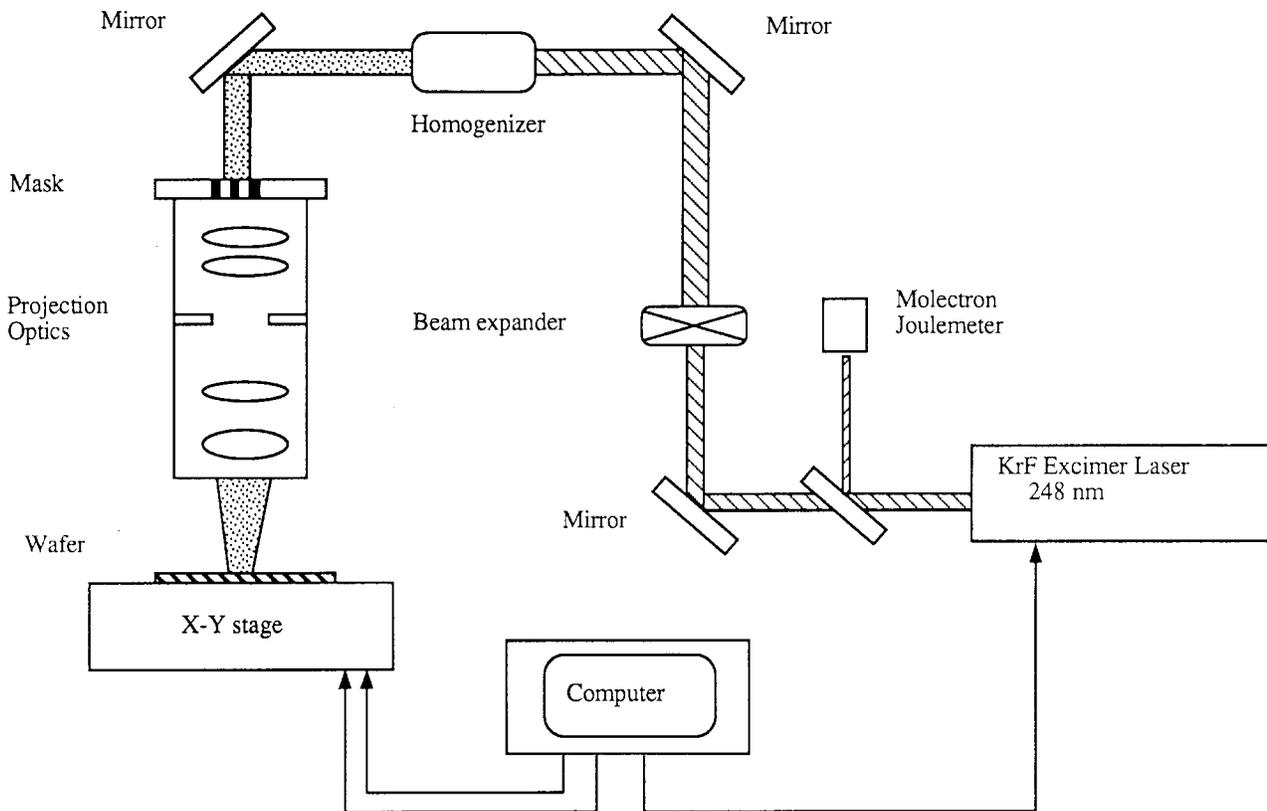
Fig. 1. Schematic diagram of an Excimer Laser Micromachining Tool designed for a manufacturing environment. Key components: an industrial-grade Lumonics Index 200 excimer laser, a beam delivery/homogenization system, a dielectric mask with micron features, a nine-element CaF_2 transfer lens for a 2:1 image reduction, and a computer-controlled five degree-freedom sample stage.

be implemented in a typical manufacturing environment with much higher fabrication efficiency and fewer process constraints.

In order to investigate the feasibility of excimer laser micromachining in an industrial environment, excimer laser micromachining of polyimide thin films deposited on silicon wafers is studied in this work. The excimer laser micromachining tool used in this study is designed to meet production demands in a manufacturing environment. While this work is focused on polyimide micromachining, the tool is nevertheless capable of machining hard ceramics and high-melting point metals. Excimer laser micromachined polyimide surface morphology is studied by scanning electron microscopy (SEM) and atomic force microscopy (AFM). After the image reduction, the cross section profiles of micromachined features ranging from 2–100 μm and surface roughness are examined by a Tencor surface profilometer. The linearity between the etch depth and the number of laser pulses is studied to ensure precise measurement and control of the etch rate when multiple laser pulses are used. The etch rate dependence on the laser fluence is investigated below and above the ablation threshold, in order to reveal a fundamental understanding of the laser interaction with polyimide films. Two polyimide thin films on crystalline silicon wafers annealed at 100 °C and 400 °C which correspond to soft baking and hard-baking temperatures, respectively, are micromachined over the same range of laser fluences in order to investigate the micromachining process for both soft-baked and hard-baked films. The difference can be

attributed to the possible physical and chemical changes in the polyimide films that may alter the absorption characteristics at the laser wavelength, $\lambda = 248$ nm. For laser fluences below the ablation threshold, the etch rate is conventionally regarded as fractional of monolayer. A limited number of studies have been conducted in this range [18], [19]. This work provides a detailed investigation on the etch rate behaviors below the ablation threshold, thereby allowing better understanding of the statistical meaning of the etch rate per laser pulse. Since the excimer laser etch rate of the polyimide film near the ablation threshold is of the order of 1 Å/pulse at the laser fluence of 100 mJ/cm^2, micromachining at the nano-scale can be realized by the laser interaction with the polyimide thin films which could have a significant impact on the rapid development in nanotechnologies such as optical data storage and nanotribology.

II. SYSTEM DESIGN AND OPTICAL ALIGNMENT

The excimer laser projection micromachining tool includes an industrial-grade Lumonics Index 200 excimer laser [3], [20], a beam delivery/homogenization system, a dielectric mask with micron features, a nine-element CaF_2 transfer lens for a 2:1 image reduction, and a computer-controlled five degree-freedom sample stage, as shown in Fig. 1. The overall design strategy for the excimer micromachining tool is to use the excimer laser beam to project the mask image on the wafer surface. By changing the laser charging voltage, the

Cylindrical Lens Arrays

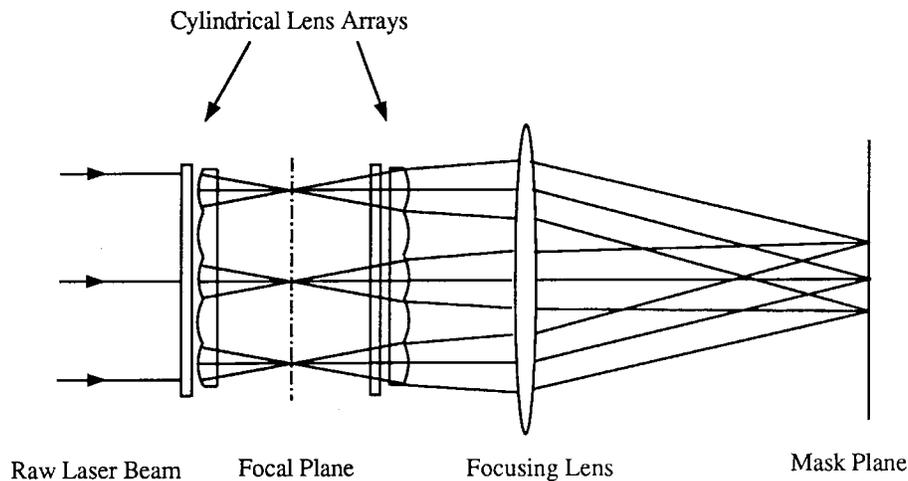Raw Laser Beam — Focal Plane — Focusing Lens — Mask Plane

Fig. 2. Schematic diagram of a fly's-eye type homogenizer consisting of two cylindrical lens arrays and showing the optical path forming a uniform spot on the mask plane.

laser fluence at the image plane can be varied. The excimer laser used in this micromachining tool has a maximum pulse energy of 400 mJ at the UV wavelength of 248 nm. The laser can operate at 1–300 Hz with 26 ns FWHM. The working medium is a premix of KrF and He gases at a pressure of 4000 mbar. A pyroelectric detector monitors the laser beam energy both at the laser exit and the image plane, yielding the integrated laser fluence over the pulse width. In order to understand the transient physical and chemical changes on the surface, the accurate knowledge of the laser beam temporal profile is essential. This profile can be acquired by a PIN silicon diode and oscilloscope with nanosecond resolution. The 10% portion of the laser beam reflected from the quartz plate tilted at an angle of 45° as shown in Fig. 1, is detected by a Molectron J50 joulemeter. The reflected laser fluence is fairly insensitive for tilt angles around 45°, thus enabling more accurate laser fluence measurements. A calibration is carried out between the image plane and the laser beam exit, so that instantaneous monitoring of the laser fluence at the image plane can be achieved to provide quality control on the excimer laser micromachining process.

The beam delivery system includes several optical and mechanical components shown in Fig. 1. Two 3″ dielectric thin film coated UV mirrors are used to reflect the laser beam upward into a 3.5× cylindrical telescope which is mounted on a two-dimensional (2-D) micrometer stage. The beam is expanded along the low-divergence direction by the telescope and does not affect the high-divergence distribution. A 3″ dielectric mirror directs the square shaped beam horizontally into a fly's-eye type beam homogenizer. As shown in Fig. 2, the fly's-eye type homogenizer consists of two arrays of cylindrical lenses which are parallel to each other. The spatially nonuniform incoming laser beam is first divided into many bundles which form arrays of point images when focused on a plane. The laser light is further diverged by a second array of cylindrical lenses and then re-focused by a spherical lens. The well-mixed laser light bundles form a uniform spot on the mask plane which then projects the mask image on the wafer surface. The width and height of the focused spot at the

mask plane can be adjusted by changing the spacing between the cylindrical lens arrays inside the homogenizer. An iris is used after the beam homogenizer to cut-off the large angle scattering light rays as well as for beam alignment. The laser beam after the homogenizer is reflected by a 3″ dielectric mirror in order to direct the beam downward to the mask plane. This mirror can be digitally tilted and translated by a computer-driven motor so that the laser beam can scan in a full wafer scale.

There are two ways commonly used for masking the laser beam: absorption and reflection. Because of the strong absorption of the UV irradiation, metal masks tend to be thermally damaged (by mechanisms such as sputtering, melting, and/or thermal-mechanical deformation). Conventional chromium masks can not sustain higher excimer laser fluences in micromachining processes. In this work, the mask is fabricated from a dielectric thin film deposited on a fused silica substrate (Balzers Corp.). The dielectric thin film is designed in such a way that the masked part reflects most of the laser energy at the specific wavelength of 248 nm, so that the thermal damage induced on the mask is greatly suppressed. Dielectric masks are far more resistant than chromium masks and usually can sustain fluences up to 1 J/cm². The mask patterning is carried out by standard lithography and the selective etching of dielectric thin film is done with ion milling. The smallest feature on the mask used in this work is about 4 μm, generating a feature of 2 μm on the wafer by the 2:1 reduction laser projection system. The mask has a 2″× 2″ active region where the repeated patterns are located.

The most important and delicate part in this micromachining tool is the nine-element CaF_2 transfer lens which projects the mask image down to the wafer with a 2:1 reduction shown in Fig. 3. The design of this transfer lens system is a complicated and challenging task. The lenses are fabricated from single crystal CaF_2 and coated with anti-reflection thin film MgF_2/Al_2O_3 designed for the 248 nm wavelength. Compared with the fused silica lens, the CaF_2 lens is much more resistant to bulk color center formation during prolonged high repetition rate operation at higher fluences [21]–[23].

Homogenized Laser Beam

Condenser Pair

Mask

Transfer Lenses

Aperture Stop Reticle
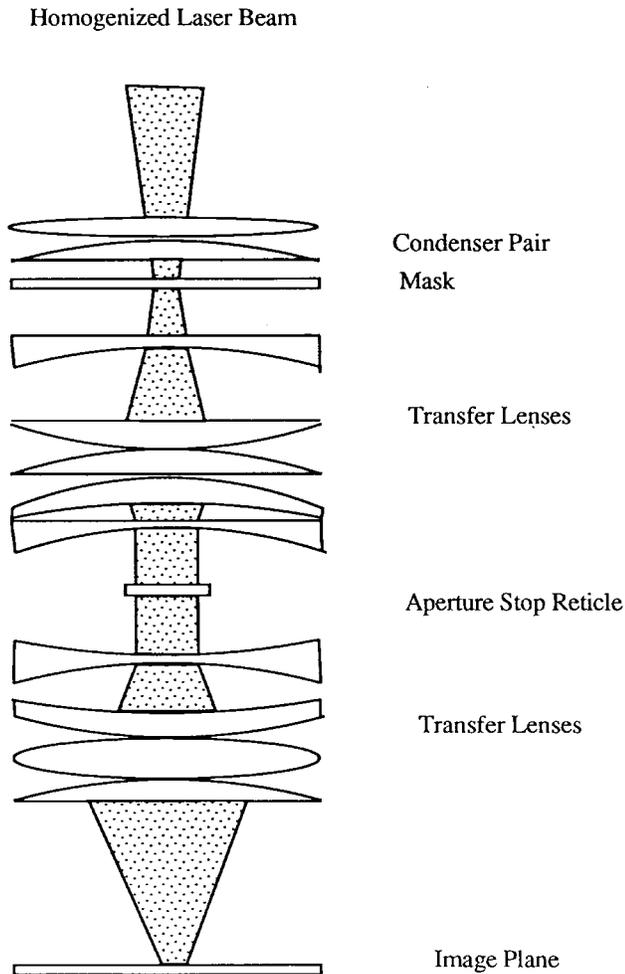
Transfer Lenses

Image Plane

Fig. 3. A nine-element CaF_2 transfer lens system with 2:1 image reduction ratio for mask projection. Key components: condenser lens pair, transfer lens, and aperture stop reticle.

Several design issues have to be addressed in optimizing the optical performance. Firstly, since any positive lens placed after the beam homogenizer forms a real image of the virtual source array, this image should form at the aperture stop of the transfer lens. It must be realized that the images should form sufficiently far away from the closest lens surface to prevent optical damage. The optical design should be therefore constrained with maintaining a larger airspace in the middle of the transfer lens where the aperture stop is located. Secondly, a single condenser lens has too much spherical aberration to keep the hot spots localized at the aperture stop plane when the illumination spot is scanned off-axis. This problem is overcome by splitting the condenser into a doublet to correct for spherical aberration. Thirdly, as the beam scans off-axis, the virtual point sources also appear to move. This movement can lead to overfilling the lenses downstream of the aperture stop. However, it can be compensated by adopting a "controlled tilt" scheme, via which the dielectric mirror tilt is controlled in order to force that the virtual point sources remain fixed in space. The transfer lens system is mounted on a 303 stainless steel housing since its thermal expansion coefficient ($17.3 \times 10^{-6}/°C$) matches that of CaF_2 ($18.7 \times 10^{-6}/°C$). The main lens housing barrel consists of three interlocking parts.

The top and bottom sections have datum surfaces that are accurately parallel to each other and perpendicular to the optical axis. Two novel features were incorporated into the mechanical design. First, provisions were made for removing the aperture stop reticle. The reticle holds two fused silica windows with a piece of UV film sandwiched in between. By exposing the film at a low laser fluence, the hot spot images at the aperture stop are recorded. This is also a good way for checking the alignment of the optical system. The second novel feature is a purge port and a network of flow channels that allows all air spaces in the transfer lens to be purged of oxygen if it is desired to prevent ozone formation inside the lens assembly. Such formation of ozone could possibly attack the anti-reflection coating and the CaF_2 lens, during prolonged KrF laser operation in the manufacturing environment. The transfer lens column position can be adjusted in the vertical direction by a micrometer, in order to achieve the best focus on the wafer surface.

The sample stage has five degrees of freedom: two angular θ tilts, $x–y$ translation and a φ rotation. The $x–y$ translation is achieved by two stepmotors with a half micron resolution. A Kensington controller is used to control the $x–y$ translations and the scanning of the dielectric mirror above the mask. Manual control has three speed selections, while computer control can be more sophisticated over the designed scan ranges and speeds. Full wafer scan can be carried out by combination of mirror scanning and $x–y$ sample stage translation. A blower and vacuum suction assembly placed close to the working surface is designed to remove laser ablated debris from the laser generated plume. The excimer laser triggering can be remote controlled either manually or computer-synchronized with the control of the stage translations and mirror scanning. Therefore, real-time integrated micromachining can be realized with computer aided design (CAD). In designing this micromachining tool, the optimization of the optical and the mechanical design is essential for improving the system performance.

Optical alignment is necessary to ensure that the excimer laser beam is properly delivered to the wafer surface and that the laser energy loss through the various optics is minimized. The optical alignment is performed with the aid of a visible HeNe laser beam transmitted through the rear mirror of the excimer laser cavity, coaxially with the excimer laser beam. First, by adjusting the dielectric mirrors with the telescope and homogenizer removed, the HeNe laser beam is brought through the iris perpendicular onto the mask plane and is centered into the optical axis of the transfer lens system. This alignment procedure is repeated with the telescope and beam homogenizer installed. With additional adjustments of the $x–y$ telescope translation and the cylindrical array tilt, the plano–plano spacing between the cylindrical lens arrays shown in Fig. 2 is set at 91.8 mm, which correspondingly yields a nominal excimer laser spot size of 6.0 mm at the mask plane. A UV-sensitive film is placed at the aperture stop reticle to check if the hot spot array forms at that position, and does not move as the mirror is scanned. The best focal distance between the last lens of the transfer lens system and the sample stage is determined by measuring the excimer laser etched profiles on the polyimide thin film deposited on
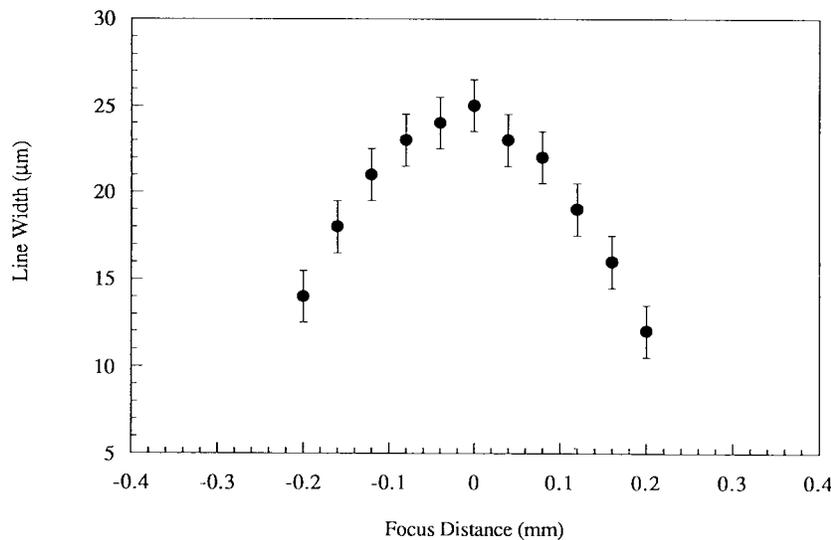
Fig. 4. Transfer lens system focus calibration with a 50-μm wide line on the dielectric mask (i.e., 25 μm line on image plane). The micromachined line-width is measured at an Alfa 200 Tencor surface profilometer. Optical field depth is about 400 μm.

the silicon wafer. The printed widths of image lines on the polyimide film at various focal distances are measured by an Alfa Tencor surface profilometer, and are depicted in Fig. 4. The best focus is obtained at a distance around 92.7 mm with the depth of field estimated at about 40 μm. The net power transmission from the excimer laser exit to the image plane is found to be about 40% by measuring the laser fluence both at the imaging plane and the laser exit. Considering the 32 lens surfaces, two mask surfaces, and four mirror surfaces (in total 38 surfaces) of the micromachining tool, an average transmission of 98% per surface is concluded. It is also found that the transmission remains constant across the full field. With the excimer laser running at 200 Hz and 275 mJ/pulse (thus delivering an average power of 55 W), 17 W reach the sample in an area of 3 mm^2. It is important to assess the system durability in a manufacturing environment. A test run demonstrated that the CaF$_2$ optics could be irradiated at 200–300 Hz for up to 75 million pulses in stationary operation (which is equal to 1.5 billion pulses in scanning operation) at 550 mJ/cm^2, with no significant deterioration in performance.

III. EXPERIMENT

The polyimide thin films studied in this work are fabricated in the Microfabrication Laboratory of the University of California at Berkeley. The 4$''$ single crystal silicon wafers are cleaned through the standard process by a Piranha solution and rinsed in DI water tanks. The native silicon dioxide on the wafer surface is removed by a diluted 10 : 1 HF solution. After 120 °C hard bake for about 1 h, the wafer is placed on a Headway spinner. The liquid polyimide (Probimide® 7020, OGC Microelectronic Materials) is applied to the wafer covering about one third of the surface. A 500 rpm spin is used to spread the liquid film onto the whole wafer. The spin-on follows at 6000 rpm for 30 s resulting in uniform thin polyimide film. A 70 °C soft-bake on a hot plate for about 6 min is used to drive the residue solvent out of the thin polyimide films. After the soft-bake, the polyimide films

are divided into two groups. One group is baked at a 100 °C hot plate for 1 h in air. The other group is annealed in a 400 °C furnace tube in a nitrogen environment for 1 h. The temperature ramp-up and ramp-down inside the tube is carefully controlled to avoid stress generation within the film. After annealing, both groups of thin films are measured by a Gaertner L116A ellipsometer and a Nanospec interferometer. The thickness of the films is determined as 5.1 μm for the films annealed at 400 °C and 9.3 μm for the film annealed at 100 °C. The uniformity of the polyimide thin films across the silicon wafer is within 7%. Surface morphology is studied using SEM and an Alfa 200 Tencor surface profilometer. The surface roughness is measured at about 30 nm; this roughness is likely due to the viscous flow of the liquid polyimide during the spin-on process. In this work, since the focus is on the study of micromachining at low and moderate fluences, the thicknesses of the polyimide thin films are larger than most of the experimentally obtained etching depths.

The thin film polyimide deposited on silicon wafer is placed on the sample stage of the micromachining tool. It is important to secure the wafer on the stage during the multiple pulses because the micron resolution could be easily ruined by slight relative motion of the wafer with respect to the stage, especially during sample stage translation. An optical microscope is used to inspect the micromachined patterns on the polyimide films and to check the focus and optical alignment. Sharpness of the micromachined patterns under the microscope provides a reasonable judgment for the focal point within 50 μm. More accurate determination of the best focus is carried out using the Tencor surface profilometer. This profilometer is capable of measuring the cross section profiles of the micromachined pattern with a few nanometer vertical resolution. A silicon p-i-n diode is used to monitor the temporal laser profile. The excimer laser fluence is measured by a Molectron J50 Joulemeter. The excimer laser is operated in the low and moderate fluence range from 10 mJ/cm^2 to 1000 mJ/cm^2. At higher laser fluences, plasma plume is generated.
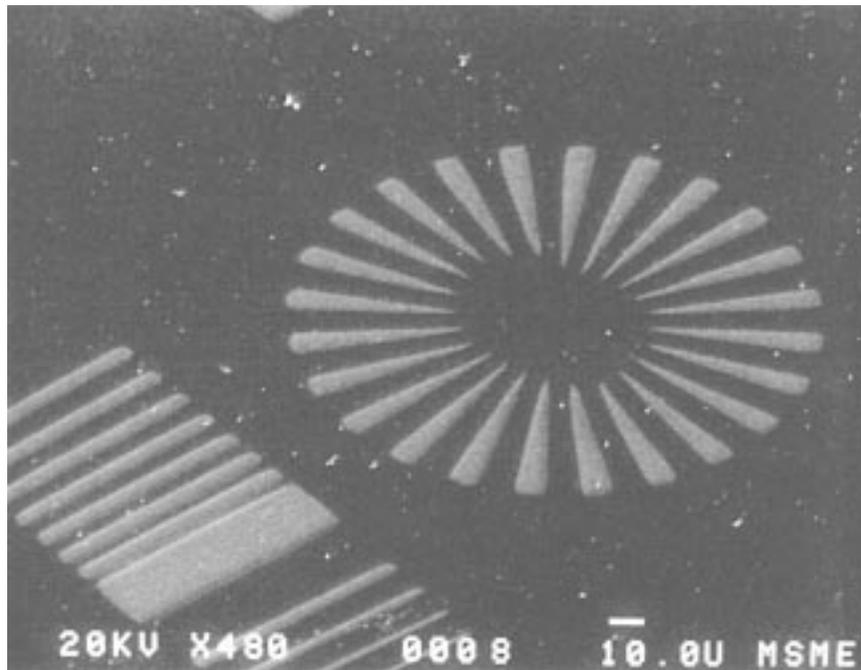
Fig. 5.   SEM of KrF Excimer laser micromachined parallel line patterns with widths from 2–25 μm and a 150 μm-diameter radiant pattern on thin film polyimide deposited on a silicon substrate and annealed at 100 °C, by five laser pulses at fluence of 400 mJ/cm^2.

Calibration of the laser fluence at the image plane is carried out by measuring the laser fluence at both the laser exit and the image plane with a 10% beam splitter (i.e., a 4″ quartz wafer). The excimer laser fluence pulse-to-pulse fluctuation is estimated at about 10%. The laser fluence is adjusted by combining the two Acton 2″ in beam splitters having transmissions of 30% and 50%, respectively, and varying the excimer laser charging voltage. At very low fluences in the range from 10–50 mJ/cm^2, an Acton 2″ in UV mirror (248 nm and 450) is used as a heavy attenuator. It is found that due to the thin film optical nature of the dielectric coating on the fused silica substrate, the transmission of the mirror can vary from 1–20% according to the incident angle of the laser beam relative to the mirror normal direction. Since these beam attenuators are placed upstream of the optical delivery system and especially of the homogenizer, the beam spatial profile at the mask plane should not be altered. The Molectron J50 Joulemeter with the detection limit of 0.1 mJ is calibrated at different energy ranges with a standard Joulemeter. A 3″ dielectric mask is placed face-up on the mask holder in order to prevent possible deposition of ablation debris onto the underlying transfer lens. Prior to the experiments, the mask is blown with a 99.99% purity nitrogen gas to ensure the micro patterns are free from dust particles.

The surface morphology and etching dynamics in the micromachining of polyimide thin film patterns are studied by several experimental techniques. SEM is used to image the micromachined polyimide thin film patterns. Since polyimide is not electrically conducting, a 100 Å Au coating is evaporated on the micromachined polyimide sample to prevent electron localization on the sample surface during the SEM operation that results in distorted images. The Tencor surface profilometer with a mechanical stylus tip of a few microns in diameter can scan the sample surface with lateral resolution of 0.1 μm, depth resolution of 1 nm, and maximum depth of 20 μm. Most previous work on excimer laser etch rate study was performed by measuring the etch depth on an etched spot with macroscopic size at least sub-millimeter. However, in this work, the etch rate measured on a microscopic 25 μm line is believed more accurate since better laser beam uniformity is expected in this scale than the millimeter scale. In order to study the etch rate at lower laser fluences, multiple laser pulses are needed to etch the polyimide surface to a reasonable depth, usually in the submicron range. Therefore, single pulse etch rates can be obtained by dividing the measured depth by the number of laser pulses incident on the polyimide films. However, it is important to verify whether the micromachined depth dependence on the number of laser pulses is linear. Two laser fluences were chosen for studying this linearity: 100 mJ/cm^2 and 200 mJ/cm^2, representing two typical laser fluences above and below the laser ablation threshold. After the linearity is confirmed, the etch rate dependence on excimer laser fluence is determined for the polyimide films annealed at 100 °C and 400 °C, respectively. The excimer laser is operated in the pulse repetition frequency range from 1–100 Hz at different laser fluences. The prolonged stationary micromachining process seems to have little effect on the definition of the micro pattern. This stability is mainly attributed to the good performance of the vibration isolation system, assembled by a 8″ thick granite tabletop placed on a pneumatic gas isolating optical table. The micromachined surface morphology is also studied by a Park Instrument AFM. A Si–N AFM tip is used to scan the micromachined surface at constant force. The AFM is operated in contact mode and the force is carefully calibrated to minimize system noise. The roughness analysis is performed on the scanned profiles for the micromachined surface as well as the virgin surface for comparison.
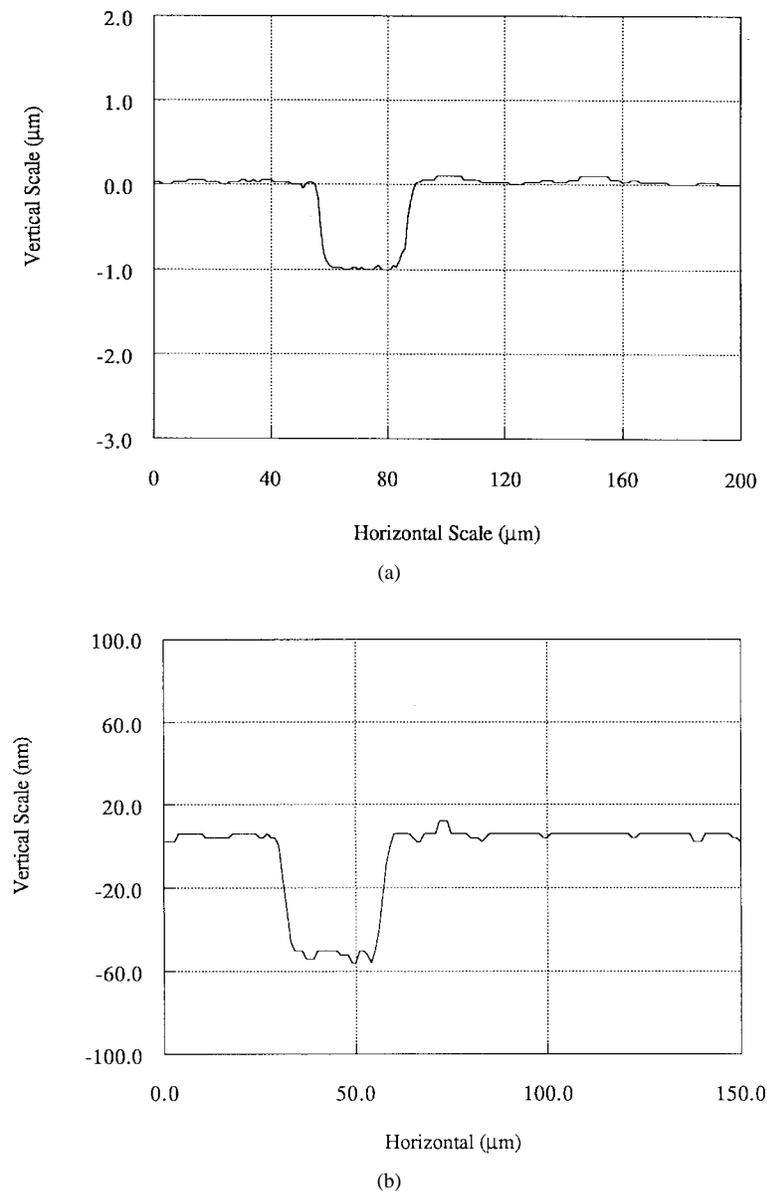
(a)

(b)

Fig. 6. Cross section profile of a 25-μm wide line etched by excimer laser projection micromachining tool with 2:1 reduction ratio. (a) 1 μm depth on polyimide thin film annealed at 100 °C by 12 pulses at laser fluence of 400 mJ/cm^2. (b) 50 nm depth on polyimide thin film annealed at 400 °C by two pulses at laser fluence of 200 mJ/cm^2.

IV. RESULTS AND DISCUSSION

The micromachined patterns on thin film polyimide deposited on a silicon substrate and annealed at 100 °C by five pulses at 400 mJ/cm^2 are observed in the SEM shown in Fig. 5. The test pattern of parallel lines with widths from 2–50 μm and the 140 μm-diameter radiant patterns are successfully imaged on the sample plane with 2:1 reduction from the mask. The straight line definition underscores the good quality of the micromachining process. The cross section profile of a 25 μm-wide line measured at Alfa 200 surface profilometer given in Fig. 6(a), shows a well-defined etch depth of 1 μm and very sharp edges. The surface and wall morphology is clean, showing little redeposition on both 100 °C and 400 °C films. It is worthwhile to note that the bottom of the micromachined 25 μm line is reasonably flat with roughness comparable

to that of the original surface. It is also observed that the micromachined surface morphology is quite similar for both films annealed at 100 °C and 400 °C, respectively. A depth of 50 nm is machined by two laser pulses at the laser fluence of 200 mJ/cm^2, as shown in Fig. 6(b). Hence, it is demonstrated that the excimer laser machining can be carried out in the nano-scale in the depth direction with good precision. Upon irradiation with higher laser fluence pulses, some areas appear slightly darkened. This darkening may have been caused by the laser ablation-induced plasma attack. A three-dimensional (3-D) AFM image of an enlarged 2 μm line with a 0.4 μm depth written by this excimer laser micromachining tool is shown in Fig. 7(a). Parallel lines of 5 μm in width and 1 μm in depth with sharp definition are also shown in Fig. 7(b). It is evident that the excimer laser micromachining tool has micron
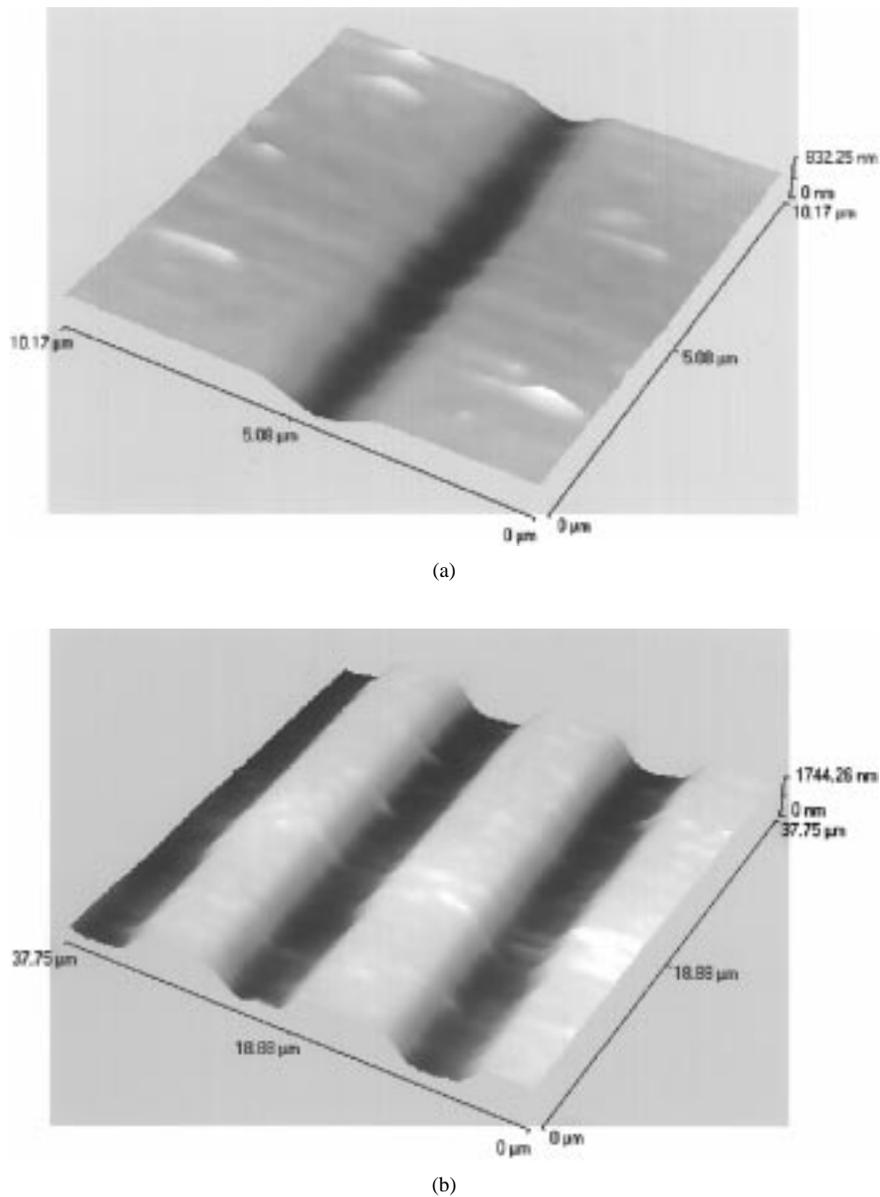
(a)

(b)

Fig. 7. 3-D Atomic Force Microscopy of (a) a line of 2 μm in width and 0.4 μm in depth micromachined by 15 pulses at laser fluence of 200 mJ/cm^2 and (b) parallel lines of 5 μm in width and 1 μm in depth micromachined by 40 pulses at laser fluence of 200 mJ/cm^2. Micromachined polyimide thin film deposited on c-silicon wafer and annealed at 400 $^\circ$C.

resolution in lateral dimensions. This result bears considerable significance for the future implementation of this direct dry etching process. The cross section of the 2 μm line AFM profile, however, shows a rounded shape instead of a sharp rectilinear-type. This is mainly attributed to the chromatic aberration of the nine-element projection optical system. The sharpness of the 4-μm line on the dielectric mask may also contribute to the resolution limit of this laser micromachining system, since the ion milling of the dielectric thin film on the mask substrate often generates some micro-cracking due to the film grain structure. Optical field depth effects are ruled out since such effects can only cause changes in the lateral dimension of the order of 1% for laser micromachining depths of about 1 μm, based on the optical field depth measurement shown in Fig. 4. Further development on opto-mechanical

design of the projection system and dry etch techniques for mask fabrication will enhance the resolution in excimer laser micromachining. It has been demonstrated recently that an excimer laser micromachining system with a self-generated-mask feature can be realized by first defining the mask patterns by direct fine single beam writing (serial writing), and subsequently, by using the finished mask for micromachining by optical projection onto the sample substrate (parallel process) [24].

Fig. 8(a) and (b) shows the etch depth dependence on the number of excimer laser pulses, at the laser fluences of 100 mJ/cm^2 and 200 mJ/cm^2 for films annealed at 100 $^\circ$C, and 400 $^\circ$C, respectively. Lines of 25 μm in width, micromachined at different laser fluences are chosen for the etch depth measurement. The linearity between the etch depth and the
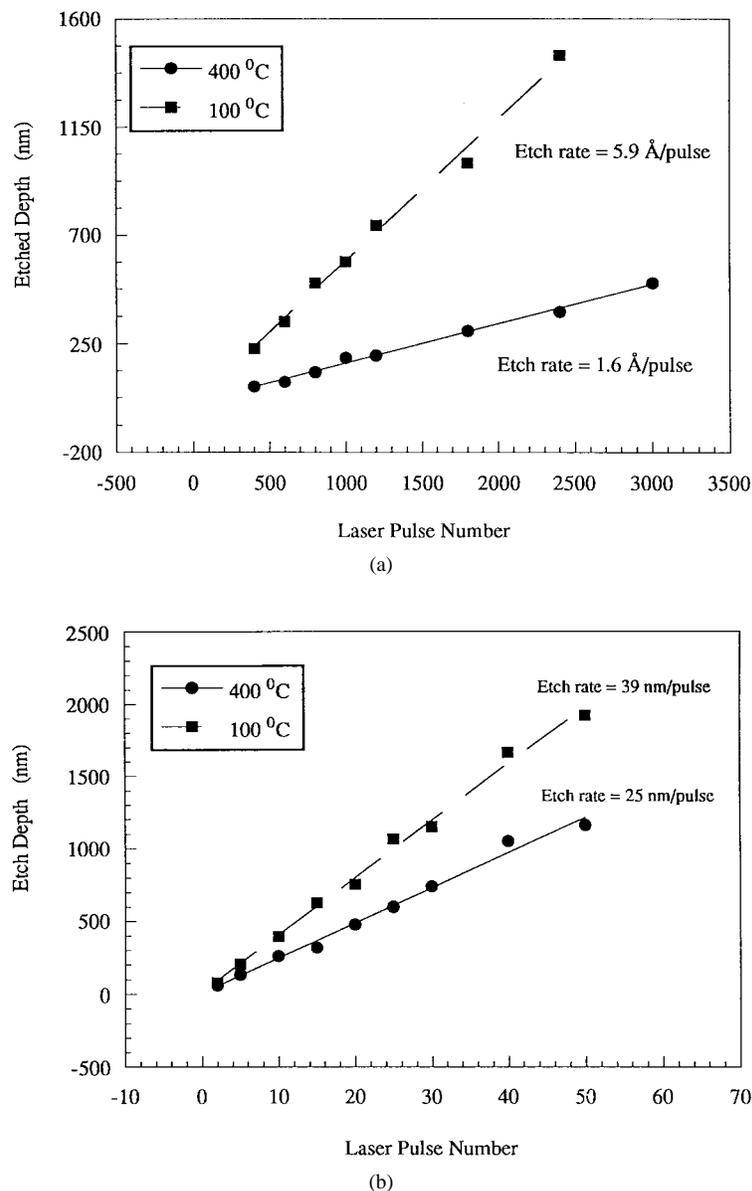
Fig. 8. Etched depth dependence on laser pulse number for a 25 μm line in excimer laser micromachining for polyimide thin films deposited on c-silicon wafer and annealed at 100 °C and 400 °C, respectively, at the laser fluence of (a) 100 mJ/cm^2 and (b) 200 mJ/cm^2.

number of the laser pulses is verified within the experimental uncertainty. The etch rate at laser fluence of 100 mJ/cm^2 is of the order of 1 Å/pulse, while the etch rate at 200 mJ/cm^2 is of the order of 10^2 Å/pulse for both films. The two orders magnitude difference in the etch rates at the two laser fluences stems from the fact that one is above the apparent laser ablation threshold, while the other is below.

The underlying mechanisms in the excimer laser interaction with polymer materials have been a subject of hot debate in the last decade [25]–[30]. Two major laser ablation mechanisms have drawn attention: the photochemical mechanism and the photothermal mechanism. These interaction mechanisms can be quite different according to the specific polymer system and laser wavelength. There have been some efforts to distinguish the two effects experimentally in the excimer laser ablation of polymer materials. However, due to the complex nature of

the problem and the often strong coupling between the two mechanisms during the transient laser ablation process, it is still hard to obtain clear evidence of the partition ratio between the two mechanisms [12]. The photochemical mechanism indicates that the electronic excitation from photon absorption in the polymer matrix can directly induce chemical bond breaking, leading to material fragmentation and ejection [15]. A theoretical model was developed to describe the photochemical ablation mechanisms [25]. This model assumes that there exists a critical, or threshold laser fluence, F_{th}, below which there are not enough broken main chain links as the rate equilibrium of the recombination of the broken chains and bond breaking is considered. As a result, the material remains in place. Above the ablation threshold, F_{th}, the decomposed fragments are ejected from the polymer matrix. Therefore, it is argued that the photochemical ablation process follows the

Beer–Lambert's law of absorption

$$F = F_0 e^{-az} \qquad (1)$$

where F_0 and F indicate the laser fluence at the material surface and at distance of z, respectively. α is the absorption coefficient and z is the distance from the surface into material. The etch depth per pulse, z_f, can be easily obtained from (1) as

$$z_f = \frac{1}{\alpha} \ln \frac{F_0}{F_{th}}. \qquad (2)$$

This photochemical ablation mechanism predicts the existence of a laser fluence threshold and a linear relationship between the etch rate and the logarithm of the laser fluence. The photothermal mechanism, on the other hand, implies that the electronic excitation from the photon energy is converted to vibrational or thermal energy in the polymer matrix before the onset of ablation [27], [28]. The material ablation occurs as pyrolytic decomposition of polymer chains at the elevated temperature. The photothermal model describes the etch rate dependence on the polymer surface temperature as

$$R = R_0 \exp \left(-\frac{E_a}{k_B T} \right) \qquad (3)$$

where R_0 is the frequency factor, E_a is the activation energy, T is the surface temperature, and k_B is Boltzmann constant. The photothermal model suggests no distinct ablation threshold and predicts that the ablation yield-fluence curve follows an "S" shape [28]. However, the induced photoablation process in the polymer materials by excimer laser may not necessarily be purely photothermal or photochemical. The combination of the two mechanisms may be present in all stages of the photoablation [29], [30]. Understanding of the physics and the chemistry involved in the photoablation of polymers is a challenging task for sorting out the two mechanisms in future research. In this work, Fig. 9(a) shows the etch rate dependence on the excimer laser fluence for polyimide films annealed at 100 °C and 400 °C. It can be seen that the etch rate increases dramatically when the laser fluence exceeds the clearly defined ablation thresholds which is about 100 mJ/cm^2 for both polyimide films. The confirmation of the linear relationship between the etch rate and the logarithm of the laser fluence above the ablation threshold for polyimide films annealed at 100 °C and 400 °C, respectively, shown in Fig. 9(a), supports the photochemical mechanism in the excimer laser ablation of polyimide films. Furthermore, the fact that the ablation thresholds for films annealed at different temperatures coincide at 100 mJ/cm^2, again suggests the photochemical nature of the excimer laser-induced ablation of the polyimide films. Optical refractive indices n and k at $\lambda = 248$ nm measured by a spectroscopic ellipsometer are listed in Table I. The n and k values for the 100 °C-annealed film are quite different than those for the 400 °C-annealed film, resulting in absorption coefficient α 82% higher in the 400 °C-annealed film than that in the 100 °C-annealed film. Reflectivities at 248 nm are found 8% for the 100 °C-annealed film and 13% for the 400 °C-annealed film. Based on measured laser ablation threshold F_0 and absorption coefficient α, the ablation depths at fluence $F = 200$ mJ/cm^2 are calculated from

TABLE I
OPTICAL PROPERTIES OF POLYIMIDE FILMS ANNEALED AT
100 °C AND 400 °C COMPARED WITH KAPTON FILM

	Polyimide film annealed at 100°C	Polyimide film annealed at 400°C	Kapton films
n	1.726	1.96	1.95 [31]
k	0.28	0.51	0.63 [31]
α (10^5/cm)	1.42	2.58	2.6 [32]
			2.2, 1.6 [33]
			3.2 [31]

TABLE II
ETCH RATE ON POLYIMIDE FILMS ANNEALED AT 100 °C AND 400
°C AT LASER FLUENCE 200 mJ/cm^2: COMPARISON BETWEEN
EXPERIMENTAL VALUES AND CALCULATED VALUES BASED ON (2)

	Polyimide film annealed at 100°C	Polyimide film annealed at 400°C
Experimental etch rate	39 nm	25 nm
Calculated etch rate	43 nm	22 nm

(2) for the two films. Good agreement is observed between the calculated depths and the experimental measured etch depths, shown on Table II. The etch rate for the 100 °C-annealed film is about 60% higher than that for 400 °C-annealed film as shown in Fig. 9(a). It is found due to the 82% higher absorption coefficient α in the 400 °C-annealed film than in the 100 °C-annealed film. Comparing the results in this work with the etch studies for Kapton H film [31]–[33], the absorption coefficients α for the 400 °C-annealed film and the 100 °C-annealed film are by 20% and 45%, respectively, lower than that for the Kapton H film (Table I), while the ablation threshold of 100 mJ/cm^2 for both films in this work is higher than the reported 30 mJ/cm^2 for Kapton film. The differences could be attributed to the chemical and physical differences between the two films [32]. It should be pointed out that it is not intended in this work to explore the etching behaviors in the near-threshold regime which extends over a laser fluence range of about $\Delta E = 20$ mJ/cm^2 as in [28].

The laser ablation threshold is conventionally regarded as the laser fluence below which the ablation rate is zero. It is not therefore surprising that relatively limited attention has been paid to the etching behaviors below the ablation threshold, although some physical changes have been observed on the irradiated surfaces [18], [19]. Fractional monolayer etching rates below the ablation threshold are confirmed in Fig. 9(b). It also reveals an interesting phenomenon: the etch rate dependence follows a power law $R = F^n$ when the excimer laser fluence drops below the ablation threshold. This power law dependence cannot be explained by invoking either pure photochemical or pure photothermal mechanisms. However, consideration of the combination of these two mechanisms may unveil the true picture. The etch rate of 0.01 Å/pulse measured by averaging multiple pulses at the laser fluence of 10 mJ/cm^2 represents only statistical meaning in micromachining. When the laser fluence is below the ablation threshold, virtually only the first surface monolayer is vulnerable to ablation, with the ablated part being fractional
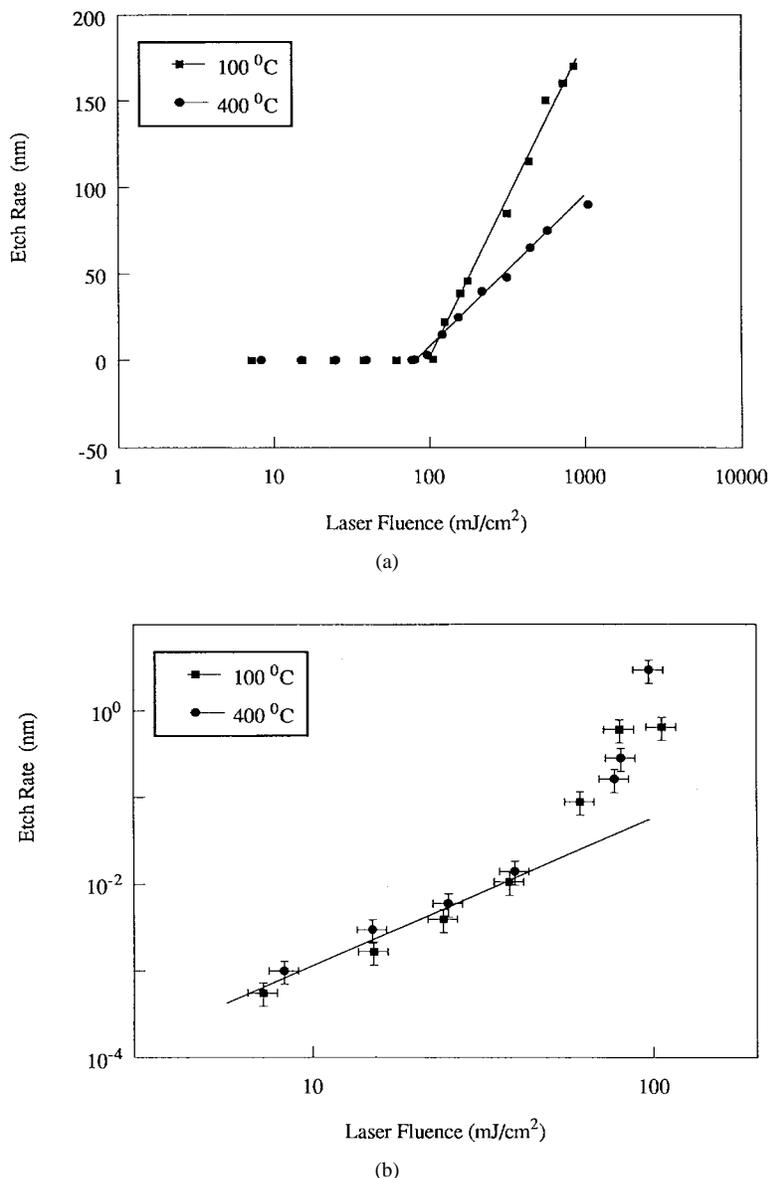
Fig. 9. Etch rate dependence on laser fluence for polyimide thin films deposited on c-silicon wafer and annealed at 100 °C and 400 °C, respectively. (a) Overall fluence range from 10–1000 mJ/cm^2 with laser ablation thresholds at 100 mJ/cm^2 and (b) below threshold fluence range from 10–100 mJ/cm^2.

of the monolayer. Although the etch rates above the ablation threshold are different by a factor of two for the two films annealed at 100 °C and 400 °C, it is found that the etch rates below the ablation threshold are almost identical for these two films. This may imply that the statistical main chain link rupture in this monolayer of the polyimide at laser below threshold fluences is largely determined by the quantum yield corresponding to the 248 nm laser wavelength or 5 eV photon energy and the photon flux, rather than the annealing temperature whose variation may cause absorption coefficient changes. Study of the photo-chemical dynamics in molecular chain session during the interaction of polymer surface and laser irradiation at low fluences would further broaden understanding of this phenomenon.

V. SUMMARY

Excimer laser projection micromachining of polyimide thin films in air is studied in this work. A KrF excimer laser projection micromachining tool with micron resolution and 2:1 reduction ratio has been designed and implemented for one-step dry etching application in microelectronics and micromechanics. This micromachining tool includes an industrial-grade excimer laser, beam homogenization and delivery system, nine-element CaF$_2$ transfer lenses, and a computerized sample stage with five degrees of freedom. Micromachined morphology of the polyimide surface is studied by SEM, AFM, and a surface profilometer. Well-defined lines of 2–50 μm with sharp edges are successfully micromachined by this excimer laser micromachining tool. It is demonstrated that etching depths as shallow as 50 nm in depth can be finely controlled through the laser fluence level and number of the laser pulses. The polyimide films are annealed at 100 °C and 400 °C, respectively, in order to study the annealing temperature effect on the excimer laser micromachining process. The etch depth dependence on the laser pulse number is found to be linear at and above the laser ablation thresholds for polyimide films annealed at

100 °C and 400 °C, respectively. Measurement of the optical properties n and k using a spectroscopic ellipsometer reveals that the absorption coefficient α for 400 °C film at 248 nm is 82% higher than that for the 100 °C-annealed film. This is found responsible to the fact that the 60% higher etch rate for 100 °C-annealed film than that of 400 °C-annealed film, found experimentally in this work. The etch rate dependence on laser fluence indicates the existence of identical ablation thresholds for both films at 100 mJ/cm^2. Linear relationships between the etch rate and $\ln(F)$ are found above laser ablation thresholds, supporting the photochemical mechanisms in laser ablation of polyimide films. However, below the laser ablation threshold, a power law dependence of the etch rate on laser fluence is revealed, which cannot be explained by solely invoking photothermal or photochemical mechanisms.

ACKNOWLEDGMENT

REFERENCES

[1] D. J. Ehrlich, "Application of laser in microelectronics and micromechanics," in *NATO ASI Series E: Applied Science, Excimer Lasers,* L. D. Laude, Ed. Amsterdam, The Netherlands: Kluwer, 1994, vol. 265, pp. 307–317.

[2] E. W. Becker, W. Ehrfeld, P. Hagmann, A. Maner, and D. Münchmeyer, "Fabrication of microstructures with high aspect ratios and great structural heights by synchrotron radiation lithography, galvanoformation, and plastic moulding," *Microelectron. Eng.,* vol. 4, pp. 35–36, 1986.

[3] F. G. Bachmann, "Industrial laser applications," *Appl. Surf. Sci.,* vol. 46, pp. 254–263, 1990.

[4] H. K. Tönshoff and J. Mommsen, "Process of generating of 3D-microstructures with excimer lasers," in *NATO ASI Series E: Applied Science, Excimer Lasers,* L. D. Laude, Ed. Amsterdam, The Netherlands: Kluwer, 1994, vol. 265, pp. 221–236.

[5] R. Patzel and H. Endert, "Excimer laser—A reliable tool for micro-processing and surface treatment," *Proc. AIP,* vol. 288, pp. 613–618, 1993.

[6] J. H. Brannon, "Micropatterning of surfaces by excimer laser projection," *J. Vac. Sci. Technol.,* vol. B7, no. 5, pp. 1064–1071, 1989.

[7] Y. Horiike, N. Hayasaka, M. Sekine, T. Arikado, M. Nakase, and H. Okano, "Excimer-laser etching on silicon," *Appl. Phys.,* vol. A44, pp. 313–322, 1987.

[8] M. Rothschild and D. J. Ehrlish, "A review of excimer laser projection lithography," *J. Vac. Sci. Technol.,* vol. B6, pp. 1–17, 1988.

[9] H. M. Phillips, S. Wahl, and R. Sauerbrey, "Submicron electrically conducting wires produced in polyimide by ultraviolet laser irradiation," *Appl. Phys. Lett.,* vol. 62, no. 20, pp. 2572–2574, 1993.

[10] R. Srinivasan and B. Braren, "Ultraviolet laser ablation of organic polymers," *Chem. Rev.,* vol. 89, pp. 1303–1306, 1989.

[11] S. Lazare and R. Srinivasan, "Surface properties of poly(ethylene terephthalate) films modified by far-ultraviolet radiation at 193 nm (laser) and 185 nm (low intensity)," *J. Phys. Chem.,* vol. 90, pp. 2124–2131, 1986.

[12] D. J. Krajnovich and J. E. Vázquez, "Formation of 'intrinsic' surface defects during 248 nm photoablation of polyimide," *J. Appl. Phys.,* vol. 73, no. 6, pp. 3001–3008, 1993.

[13] J. R. Lankard, Sr. and G. Wolbold, "Excimer laser ablation of polyimide in a manufacturing facility," *Appl. Phys.,* vol. A54, pp. 355–359, 1992.

[14] F. Bachmann, "Excimer laser in a fabrication line for a highly integrated printed circuit board," *Chemtronics,* vol. 4, pp. 149–152, 1989.

[15] R. Srinivasan, "Kinetics and the ablative photodecomposition of organic polymers in the far ultraviolet (193 nm)," *J. Vac. Sci. Technol.,* vol. B1, no. 4, pp. 923–926, 1983.

[16] Lambda Physik, *Highlights,* no. 42, Nov. 1993.

[17] X. Wen, D. Hare, and D. D. Dlott, "Laser polymer ablation threshold lowered by nanometer hot spots," *Appl. Phys. Lett.,* vol. 64, no. 2, pp. 184–186, 1994.

[18] J. Heitz, E. Arenholz, D. Bauerle, H. Hibst, A. Hagemeyer, and G. Cox, "Dendritic surface structures on excimer-laser irradiated PET foils," *Appl. Phys.,* vol. A56, pp. 329–333, 1993.

[19] E. Arenholz, V. Svorcik, T. Kefer, J. Heitz, and D. Bauerle, "Structure formation in UV-laser ablated poly-ethylene-terephthalate (PET)," *Appl. Phys.,* vol. A53, pp. 330–331, 1991.

[20] J. R. Lankard, Sr., "What industry needs in a high power excimer laser," *Proc. SPIE,* vol. 1377, pp. 2–5, 1990.

[21] D. J. Krajnovich *et al.,* "Testing of the durability of single-crystal calcium fluoride with and without antireflection coatings for use with high-power KrF excimer laser," *Appl. Opt.,* vol. 31, pp. 6062–6075, 1991.

[22] W. P. Leung, M. Kulkarni, D. Krajnovich, and A. C. Tam, "Effect of intense and prolonged 248 nm pulsed-laser irradiation on the properties of ultraviolet-grade fused silica," *Appl. Phys. Lett.,* vol. 58, pp. 551–553, 1991.

[23] D. J. Krajnovich, I. K. Pour, A. C. Tam, W. P. Leung, and M. K. Kulkarni, "248 nm lens materials: Performance and durability issues in an industrial environment," *Proc. SPIE,* vol. 1848, pp. 544–560, 1992.

[24] H. Schmidt, J. Ihlemann, and B. Wolff-Rottke, "Excimer laser microma-chining based on dielectric masks," *Proc. SPIE,* vol. 2246, pp. 67–73, 1994.

[25] H. H. G. Jellinek and R. Srinivasan, "Theory of etching of polymers by far-ultraviolet pulsed laser and long-term irradiation," *J. Phys. Chem.,* vol. 88, no. 14, pp. 3048–3051, 1984.

[26] D. D. Dlott, "Ultrafast vibrational energy transfer in the real world: Laser ablation, energetic solids, and hemeproteins," *J. Opt. Soc. Am. B,* vol. 7, no. 8, pp. 1638–1652, 1990.

[27] D. P. Brunco, M. O. Thompson, C. E. Otis, and P. M. Goodwin, "Temperature measurements of polyimide during KrF excimer laser ablation," *J. Appl. Phys.,* vol. 72, no. 9, pp. 4344–4350, 1992.

[28] S. Küper, J. Brannon, and K. Brannon, "Threshold behavior in polyimide photoablation: Single-shot rate measurements and surface-temperature modeling," *Appl. Phys.,* vol. A56, pp. 43–50, 1993.

[29] B. Luk'yanchuk, N. Bityurin, S. Anisimov, and D. Bauerle, "The role of excited species in UV-laser materials ablation: I. Photo-physical ablation of organic polymers," *Appl. Phys.,* vol. A57, pp. 367–374, 1993.

[30] D. Bauerle, B. Luk'yanchuk, N. Bityurin, and S. Anisimov, "Pulsed-laser ablation," in *NATO ASI Series E: Applied Science, Excimer Lasers,* L. D. Laude, Ed. Amsterdam, The Netherlands: Kluwer, 1994, vol. 265, pp. 39–57.

[31] E. T. Arakawa, M. W. Williams, J. C. Ashley, and L. R. Painter, "The optical properties of Kapton: Measurement and application," *J. Appl. Phys.,* vol. 52, no. 5, pp. 3579–3582, 1981.

[32] G. Koren and J. T. C. Yeh, "Emission spectra and etching of polymers and graphite irradiated by excimer lasers," *J. Appl. Phys.,* vol. 56, no. 7, pp. 2120–2126, 1984.

[33] J. H. Brannon, J. R. Lankard, A. I. Baise, F. Burns, and J. Kaufman, "Excimer laser etching of polyimide," *J. Appl. Phys.,* vol. 58, no. 5, pp. 2036–2043, 1985.

Xiang Zhang received the B.S. and M.S. degrees in physics from Nanjing University, China, in 1985 and 1988, respectively, the M.S. degree in mechanical engineering from the University of Minnesota, Minneapolis, in 1992, and the Ph.D. degree from the Department of Mechanical Engineering, University of California, Berkeley, in May 1996.

He was a research physicist at Fermi Accelerator National Laboratory, from 1989 to 1990. He has worked on phase transitions in ferroelectric liquid crystal, high Tc superconductivity, high energy physics, and aerosol science and technology. His current research interest includes: pulsed laser processing of advanced materials, in situ optical diagnostics in microfabrication, and process for MEMS (micro-electro-mechanical-system). He joined the Department of Industrial and Manufacturing, Pennsylvania State University, University Park, an Assistant Professor in August 1996.

Costas P. Grigoropoulos received the Diploma Degrees in naval architecture and marine engineering, and in mechanical engineering, from the National Technical University of Athens, Athens, Greece. He also received the M.Sc. degree and the Ph.D. degree, both in mechanical engineering from Columbia University, NY, in 1983 and 1986, respectively.

He joined the faculty of the Department of Mechanical Engineering, University of California, Berkeley, as an Assistant Professor in 1990, after serving as an Assistant Professor of Mechanical Engineering, University of Washington, Seattle, from 1986 to 1990. Since July 1993, he has been an Associate Professor in Mechanical Engineering. His research interests are in laser materials processing and micromachining, heat transfer in thin films, radiative and thermal properties of thin film materials, melting and vaporization phase transformations, thin film crystal growth, and thermocapillary flows.

Andrew C. Tam (M'86–SM'88) received the Ph.D. degree in physics from Columbia University, NY, in 1975.

He is a Manager of the Laser Processing Department, IBM Almaden Research Center, San Jose, CA. His research interest is in the areas of laser-materials interaction and the development of materials processing technologies, as well as optical and photothermal measurements and process monitoring techniques.

Dr. Tam is a Fellow of the American Physical Society and the Optical Society of America.

Douglas J. Krajnovich received the B.S degree in chemistry from the University of Illinois, Urbana, and the Ph.D. degree in physical chemistry from the University of California, Berkeley.

After a postdoctoral stint at Indiana University, Bloomington, he spent nine years at the IBM Almaden Research Center, San Jose, CA, working on basic and applied aspects of laser-surface interactions and laser materials processing. He is now a Senior Principal Engineer at Western Digital Corporation.